Title

Numerical and experimental validation for the thermal transmittance of windows with cellular shades

Author

Hart, Robert

Publication Date

2018-05-01

DOI

10.1016/j.enbuild.2018.02.017

Peer reviewed

Lawrence Berkeley National Laboratory

Numerical and experimental validation for the thermal transmittance of windows with cellular shades

Robert Hart

Lawrence Berkeley National Laboratory

Energy Technologies Area
2018

DOI: https://doi.org/10.1016/j.enbuild.2018.02.017

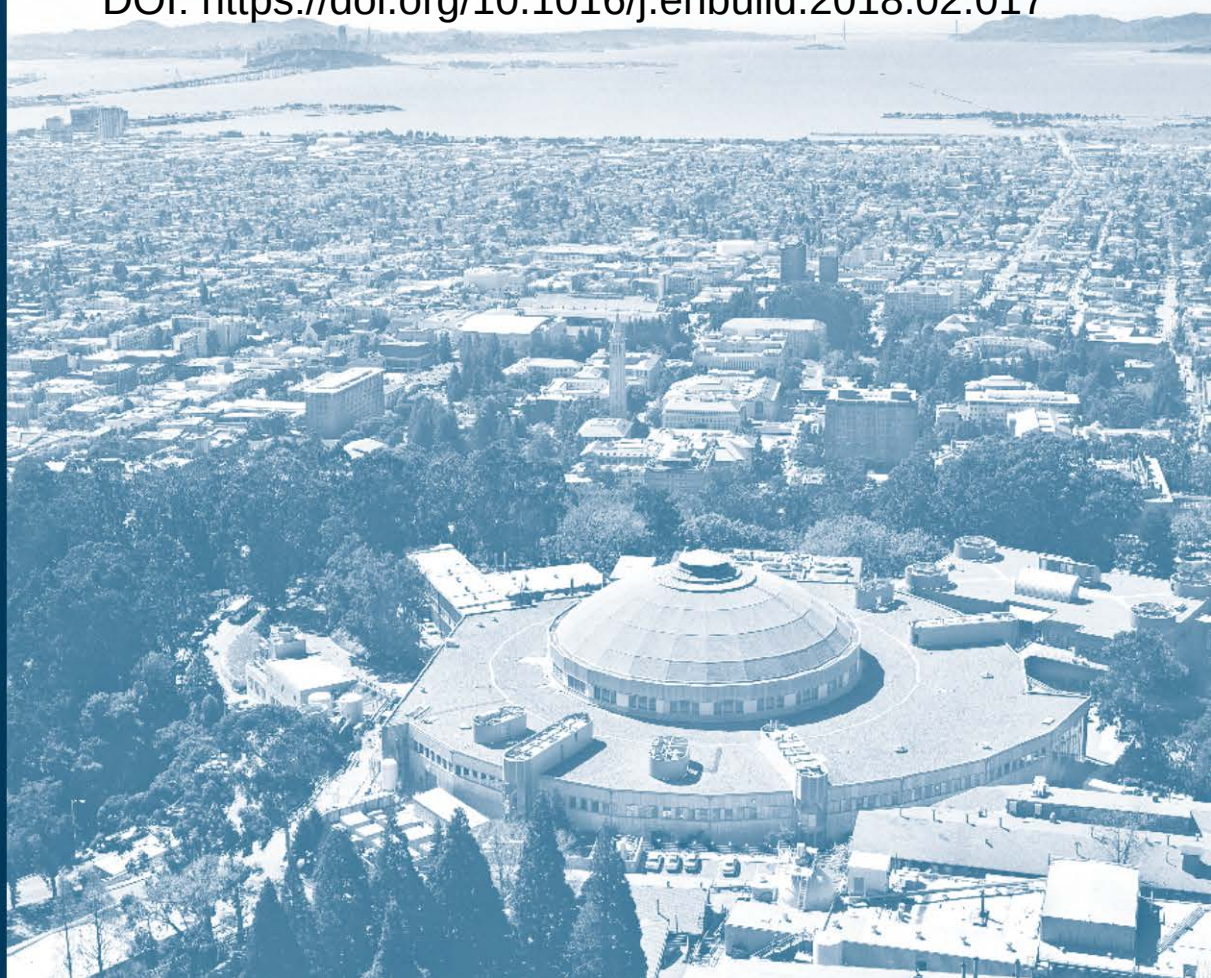

Abstract

Some highly energy efficient window attachment products are available today, but more rapid market adoption would be facilitated by fair performance metrics. It is important to have validated simulation tools to provide a basis for this analysis. This paper outlines a review and validation of the ISO 15099 center-of-glass zero-solar-load heat transfer correlations for windows with cellular shades. Thermal transmittance was measured experimentally, simulated using computational fluid dynamics (CFD) analysis, and simulated utilizing correlations from ISO 15099 as implemented in Berkeley Lab WINDOW and THERM software. CFD analysis showed ISO 15099 underestimates heat flux of rectangular cavities by up to 60% when aspect ratio (AR) = 1 and overestimates heat flux up to 20% when AR = 0.5. CFD analysis also showed that wave-type surfaces of cellular shades have less than 2% impact on heat flux through the cavities and less than 5% for natural convection of room-side surface. WINDOW was shown to accurately represent heat flux of the measured configurations to a mean relative error of 0.5% and standard deviation of 3.8%. Several shade parameters showed significant influence on correlation accuracy, including distance between shade and glass, inconsistency in cell stretch, size of perimeter gaps, and the mounting hardware.

Keywords: building energy; windows; window attachment; shading; U-factor; heat transfer; cellular shade; honeycomb shade; CFD

1. Introduction

Virtually every home in the U.S. has some form of shades, blinds, drapes or other window attachments, but few have been designed for energy savings. High performance solutions for residential and commercial window attachments therefore offer large short-term energy savings potential. Due to the wide variety of window attachment solutions, energy savings can be accomplished in all climates by utilizing systems that reduce heating energy, reduce cooling energy, or both. These products can also reduce mechanical heating and/or cooling system sizing and improve indoor thermal comfort.

Some high performance products are available today but more rapid market adoption would be facilitated by better optimization and selection criteria, e.g. fair performance comparison and rating labels. There are also opportunities to re-engineer and enhance existing products to dramatically improve their performance, both in terms of intrinsic properties and in operations.

In order to provide a common basis of comparison, and to design more cost effective high performance window attachments, it is important to have validated simulation tools. These tools enable rapid design development and optimization through the use of parametric analysis and solution optimization. Several different approaches to simulate windows with attachments have been studied and developed. The primary focus of these works has been the experimental measurement, simulation, and simplified model development of solar heat gain for horizontal (Venetian) blinds located inside glazing unit glass and in room (room side).

Relatively little research has been done to characterize the nighttime (zero solar load) U-factor impacts of attachment products other than horizontal blinds, including in-plane products such as solar screens, roller shades, insect screens, drapes, and cellular shades. Little research focused on measurements or model development for thermal transmittance of cellular shades could be found in the literature. The available works performed by Dodge (2011), Peterson (2015), and Steven Winter Associates (2008) all use systems in uncontrolled environments and minimal measurement locations; typically, one temperature sensor per surface. While informative, the results from these studies are not suitable for model development or validation.

The thermal performance of in-plane attachment products can, in general, be simulated similar to sealed (insulated) glazing with modifications to account for long-wave (IR) radiant transmission, gas flow across attachment layers, and shape factors affecting convection over the surface. Wright (2008) developed a resistance network model and van Dijk and Oversloot (2003) developed a model utilizing buoyancy driven pressure difference modifications to the surface convection coefficient of sealed cavities to account for gas flow across layers. The van Dijk model is utilized in the ISO 15099 standard (2003), WIS (van Dijk et al. 2003), and Berkeley Lab WINDOW simulation programs (Tarcog 2006). Collins and Wright (1998) showed that early implementations of this model incorrectly accounted for IR transmission through layers, but this has since been corrected in the WINDOW software. Laouadi (2009) expanded on the van Dijk/ISO 15099 model by adding product type specific correlations for equivalent properties, flow between layers, and surface coefficients.

The most common simplified model for ventilated window systems determines the surface convection coefficients based on the opening characteristics of layers adjacent to ventilated cavities. Berkeley Lab WINDOW includes several specialized window attachment models based on the ventilated window system method including: cellular shades, horizontal louvered blinds and perforated screens. In addition, the Complex Glazing Database (CGDB) contains complex attachment product optical performance data, and has been publicly released. In order to have confidence in the newly developed attachment models, they must be validated through extensive testing and detailed computational fluid dynamics (CFD) simulation. This paper outlines a review and validation of the ISO 15099 center-of-glass (COG) heat transfer correlations for cellular shades through measurement and simulation. The impact on no-solar-load system thermal transmittance due to dimensional and material variations of the shades is measured experimentally, simulated using CFD analysis, and simulated utilizing simplified correlations from ISO 15099 with the Berkeley Lab WINDOW and THERM software.

2. Methodology

Correlations to determine thermal transmittance (U-factor) of shading devices arranged parallel to the window plane are defined in ISO 15099. While the model is physically based, the standard does not cite any validation of the approach through either measurements or detailed simulation. An extensive literature review of research on heat flux through shading systems and a detailed analysis of the ISO 15099 ventilated algorithm was completed by Hart, et. al. (2017). Validation for shading devices with perimeter gaps and porous surfaces such as solar screens, roller shades, and horizontal venetian blinds was also completed in that work. Validation of the correlations as they apply to cellular shades is presented here.

The typical geometries of cellular shade cells and layers as a whole are first defined to form a basis of the product category. The methodology for simulating COG thermal transmittance utilizing the ISO 15099 correlations with these geometries within the Berkeley Lab WINDOW, THERM and Radiance framework is then presented.

Detailed CFD simulations using finite element analysis (FEA) and steady-state measurements of cellular shade systems were performed for comparison to the ISO 15099 correlations. Modifications to the Berkeley Lab software suite implementation of the correlations are proposed to provide higher correlation of measured and simulated thermal transmittance of the systems.

2.1. Geometry

Two aspects of cellular shade geometry were considered; the cells themselves and the layer as a whole. The four cell geometries considered in this work are single-cell, cell-in-cell, cell-in-cell-in-cell, and stacked double cell. These geometries are shown in Figures 1a-d. The significant dimensions include the cell width (w), cell height or pitch (p), side length (l_s), and glue-line length (l_g). The comparable side lengths were considered to be equal, as shown in Figure 1a. Cell wall thickness has insignificant impact on overall layer thermal performance for the materials considered, so a typical material thickness of 0.2 mm was

assumed. Indoor, or room-side, mounted cellular shades were studied exclusively in this work. The typical geometry relative to the glazing system is shown in Figure 1e.

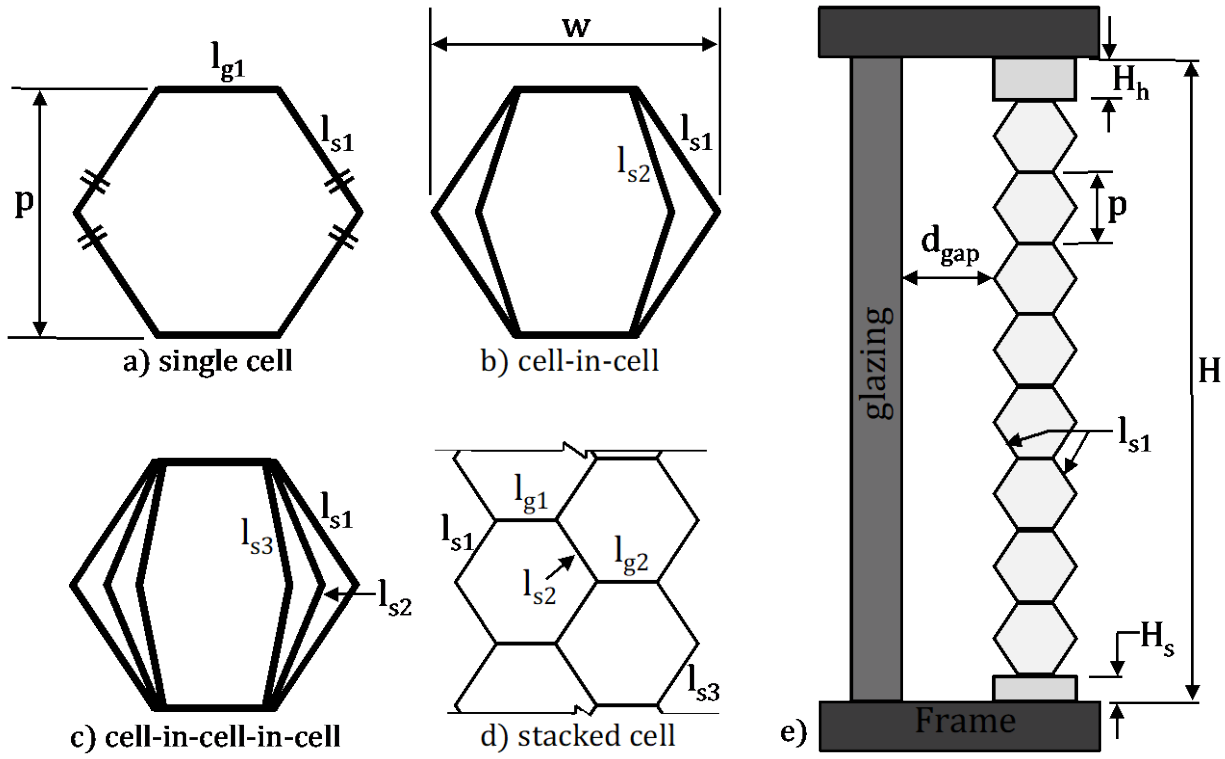

Figure 1. Geometry of a) single-cell, b) cell-in-cell, c) cell-in-cell-in-cell, d) stacked double cell, and e) side view of room-side mounted shade installed in window.

p:	Height (pitch) of cell	[m]
w:	Width of cell	[m]
H:	Height of shade	[m]
H_h:	Height of shade head rail	[m]
H_s:	Height of shade sill rail	[m]
d_{gap}:	Shade-window gap depth	[m]
l_{g1}:	Glue-line length number 1	[m]
l_{g2}:	Glue-line length number 2 (if present)	[m]
l_{s1}:	Length 1st cavity wall	[m]
l_{s2}:	Length 2nd cavity wall (if present)	[m]
l_{s3}:	Length 3rd cavity wall (if present)	[m]

2.2. Correlations

The correlations developed in ISO 15099 to predict the heat flux through window systems have been implemented in one and two dimensions with the Berkeley Lab WINDOW and THERM software programs. The process for simulating a glazing system with cellular shades utilizing the software is shown in Figure 2. First, the relevant thermal and optical material properties of glue-lines and cavity walls are entered into the Berkeley Lab WINDOW shade material database. The properties may be measured spectral data or integrated into solar, visible, and thermal infrared groups. The cellular shade geometry has significant influence on optical properties of the assembled shade layer. To enable manufacturer freedom in product design, the cell geometry is defined with two-dimensions in THERM with the cell wall properties appropriated from the previously defined shade material database. The THERM program determines the 1D equivalent thermal properties of the shading layer based on the 2D geometry.

Radiance is used for ray tracing shade layer optical properties since it can be freely distributed with the Berkeley Lab WINDOW program. The geometry and materials are converted to .RAD files and then passed into genBSDF program, which outputs bidirectional scattering distribution function (BSDF) matrices for the product as a layer. This is done for three different wavelength bands, visible (380-780 nm), solar (300-2500 nm), and thermal infrared (5-25 microns). The results from these three runs are combined into a single BSDF file that is read by Berkeley Lab WINDOW. The calculated shade layer properties are then combined with the remainder of the glazing system and boundary conditions to determine the 1D center-of-glazing thermal performance. Since the solution is solved for iteratively, the previously defined THERM cell geometry is called repeatedly to ensure accurate thermal boundary conditions during the calculation.

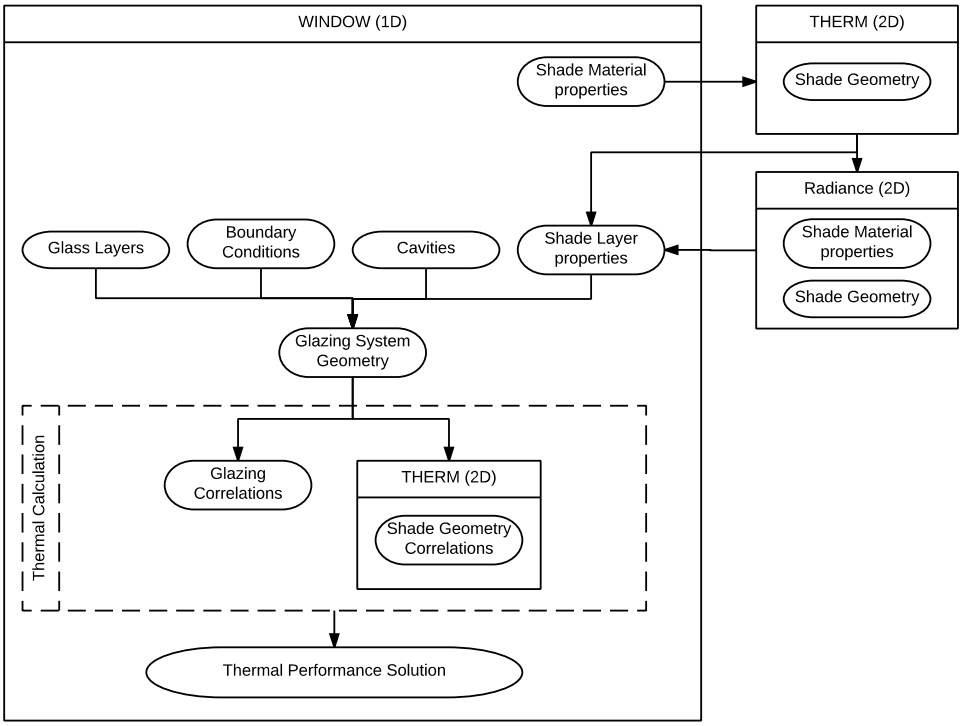

Figure 2. Cellular shade simulation algorithm flow used by Berkeley Lab WINDOW and THERM software.

2.3. Finite Element Analysis (FEA)

Heat flux through rectangular fluid filled cavities has been extensively studied by others such as El Sherbiny et al. (1982). The work by El Sherbiny et al. is the basis for the sealed cavity model in the ISO 15099 standard but several studies, such as Zhao et al. (1998) and Wright (1996), have proposed revised correlations to more closely match simulations and measurements of low Rayleigh Number (Ra) flow and high height-to-width aspect ratio (AR) cavities. Convection from wave type surfaces has been studied by Yao (1983) and Oosthuizen (2011), and Oosthuizen and Paul (2012) considered window blinds with wave type surfaces. All of these studies provide a means to calculate average heat flux based on definitions of the Nusselt (Nu) and Ra numbers as shown in equations 1-2; where Nu is the ratio of convective to conductive heat transfer across the cavity and Ra designates strength of the buoyancy driven flow. An empirical correlation between them is determined for specific geometries in the form of equation 3, where Nu is a function of the Ra number. Theory says Nu scales with $Ra^{1/4}$ for non-vented rectangular cavities and vertical flat plates with natural convection (Bejan 2004). In ISO 15099, multiple empirical correlations controlled by the cavity AR and Ra range are used in place of the theoretical scaling.

$$Nu = \frac{q \cdot L}{k \cdot \Delta T} \quad [1]$$

$$Ra = \frac{\rho^2 \cdot g \cdot C_p \cdot \beta \cdot \Delta T \cdot L^3}{k \cdot \mu} \quad [2]$$

$$Nu = f(Ra) \quad [3]$$

where:

Nu:	Nusselt number	[-]
Ra:	Rayleigh number	[-]
q:	Heat flux	[W m^{-2}]
L:	Characteristic length	[m]
k:	Thermal conductivity	[W m^{-1} K^{-1}]
T:	Temperature	[K]
ρ:	Density	[Kg m^{-3}]
g:	Gravity	[m s^{-2}]
C_p:	Heat capacity	[J kg^{-1} K^{-1}]
β:	Coefficient of thermal expansion	[K^{-1}]
μ:	Dynamic viscosity	[Pa s]

The non-dimensional form of Equations 1-3 allows for general analysis that can be applied to a wide range of geometries, fluid properties, and temperature ranges. For this reason, the parameters were non-dimensionalized for this FEA study. In the multiphysics analysis program COMSOL, the finite element method was used to solve the coupled heat and fluid-flow transient equations in two dimensions. Conduction, convection and radiation were simulated numerically with conditions typical of those shown in Figure 3, where cavity walls were held at constant temperatures T_c and T_w, top and bottom cavity walls were adiabatic, non-slip walls, and cavity fluid was initially at rest and uniform temperature. COMSOL default meshing was used to construct the computational domains. A uniform rectangular mesh was constructed with minimum criteria of two elements within the boundary layer thickness, δ, based on equation 4 for laminar flow.

$$\delta = \left(Ra\frac{1}{AR}\right)^{-0.25} \quad [4]$$

Sensitivity analysis was performed at the minimum and maximum Ra extremes to ensure that solved heat flux solutions were independent of mesh density to less than 1 percent. Viscous dissipation was not addressed and all thermophysical properties were assumed to be constant except for the buoyancy term of the y-momentum equation where the Boussinesq approximation was used. A constant Prandlt number for air of 0.71 was assumed and the parallel direct iterative sparse solver (PARDISO) was used.

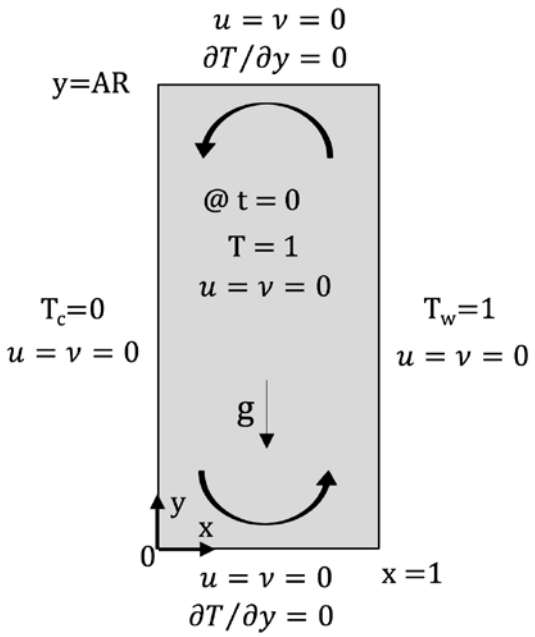

Figure 3. Representative geometry and boundary conditions for FEA of natural convection in fluid filled cavity.

Fluid heat transfer for constant temperature walls of four geometries was studied as shown in Figure 4. Geometry (a) represents the cavity between glass and cellular shade; Geometry (b) is a rectangular cell and is the baseline geometry used in the ISO 15099 correlation; Geometry (c) represents a hexagonal cellular shade cell; and Geometry (d) represents natural convection along the triangular wave surface of a cellular shade.

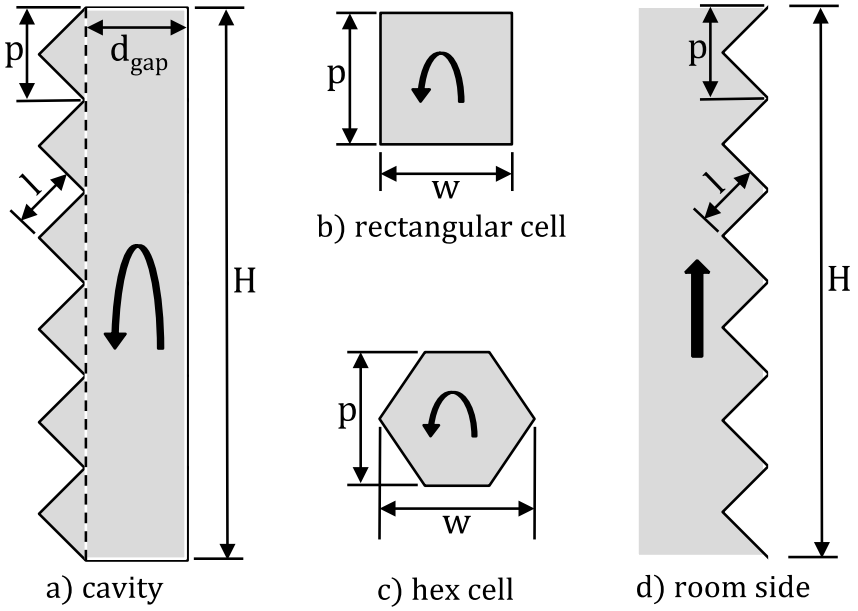

Figure 4. 2D geometries utilized in FEA simulations for fluid heat transfer with constant temperature walls. Fluid areas shown in grey.

Analysis was based on AR and a range of Ra; $10^2 \leq Ra \leq 10^7$ for cell models and $10^2 \leq Ra \leq 10^5$ for cavity models between glass and shade. Ra was based on characteristic length of cavity width. Wave surfaces were analyzed for a range of pitch, p, and side length, l, relative to cavity width, d_{gap}, of $0.10d_{gap} \leq p \leq d_{gap}$ and $0.25d_{gap} \leq l \leq d_{gap}$. Figure 5, reproduced from Chenoweth (1986), shows that only laminar flow regimes were encountered for the given parameters of this work, and therefore, turbulent flow was not considered here.

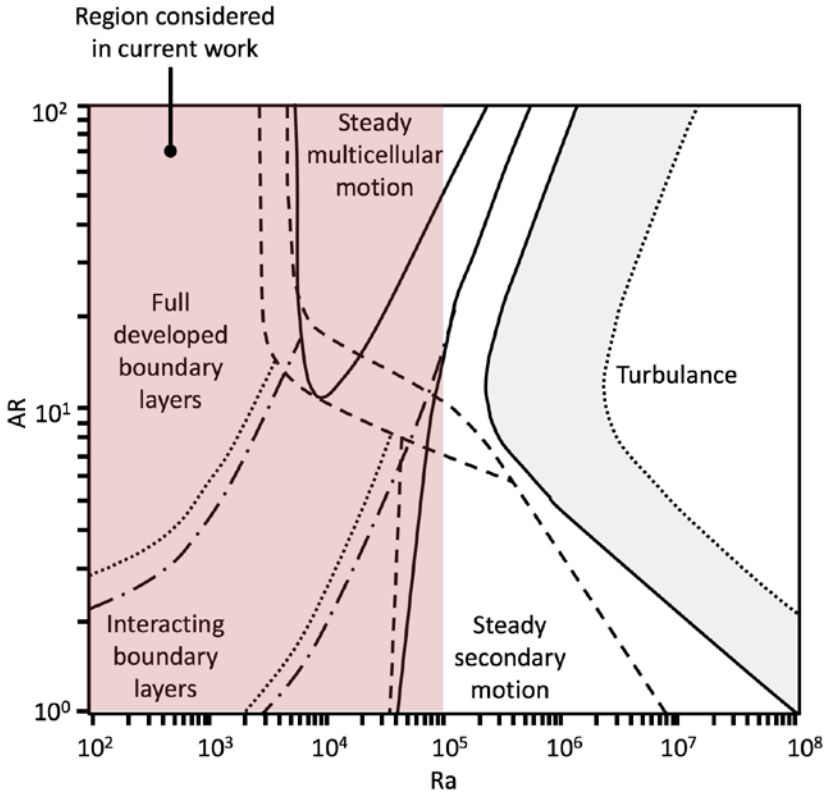

Figure 5. Flow regimes of rectangular cavities with isothermal walls based on height-to-width aspect ratio (AR). The regions encountered in this study are highlighted. The figure is reproduced from Chenoweth (1986).

2.4. Steady state measurements

Industry standard quantitative measurement of window heat flux is performed with calorimetric "hot box" instruments as outlined in ISO 12567 (ISO 2010). An alternative method utilizing calibration transfer standards (CTS) (ASTM 2014) was used for the current work. Figure 6 illustrates the test chamber configuration where the CTS and shade system were placed in the specimen plane. The forced convection chamber represents the cold, or outdoor-side, and the natural convection chamber represents the relatively

warmer indoor-side in these measurements. Natural convection on the room-side is downward under these conditions, as shown with direction arrows in the figure.

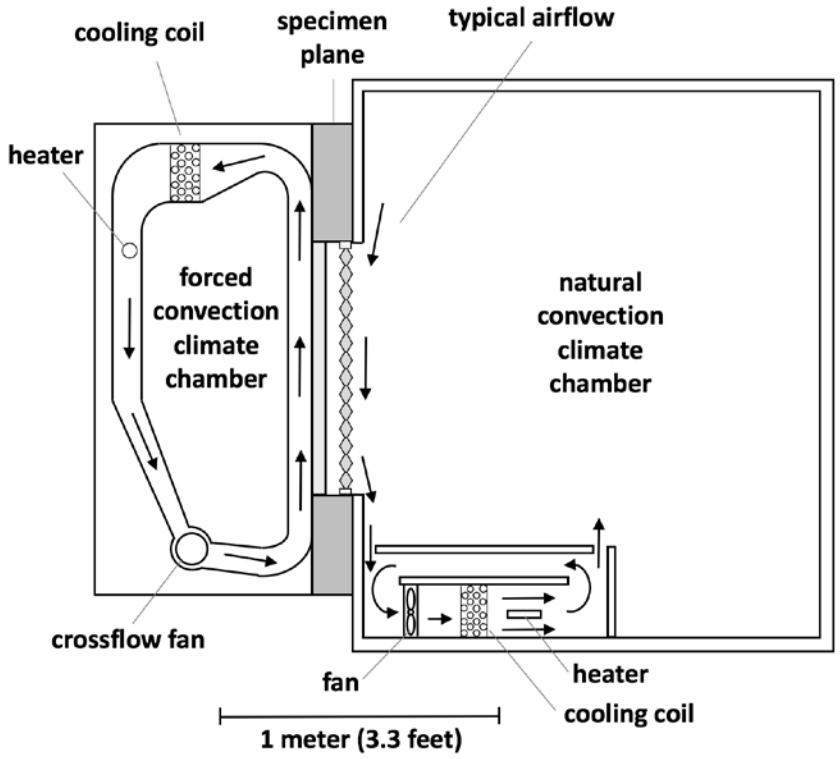

Figure 6. Schematic cross-section of environmental test chambers. CTS and cellular shade system were placed in the specimen plane.

The CTS was constructed with a foam layer sandwiched between two panes of 3 mm glass. Thermocouples were placed in a 3 x 6 grid (18 per surface) on the inside surface of two 1080 mm high, 775 mm wide, and 3 mm thick glass panes with a calibrated 12.7 mm foam layer between them. The assembled 18.7 mm thick system thermal conductivity was measured per ASTM C518 (ASTM 2017) with a Lasercomp FOX 300 heat flow meter to be 0.062 ± 0.001 $Wm^{-1}K^{-1}$. This is between the center-of-glass thermal performance of a typical 18.7 mm thick double-pane-clear IGU (effective conductivity of 0.096 $Wm^{-1}K^{-1}$) and a typical 18.7 mm thick double-pane-low-e IGU (effective conductivity of 0.045 $Wm^{-1}K^{-1}$).

The 18 temperature pair measurements allowed for calculation of local heat flux through the specimen in many locations. Figure 7 illustrates the configuration of the CTS specimen and sample shade utilized for this study, including the locations of sensing thermocouples.

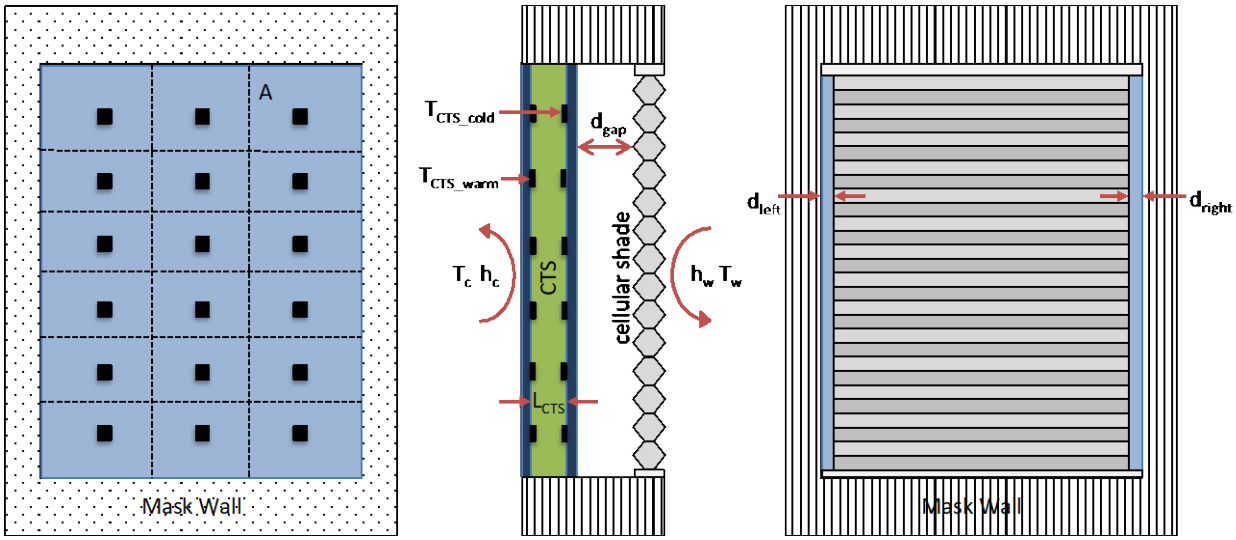

Figure 7. Back, side and front views of the CTS and cellular shade assembly in specimen mounting plane of the IR chamber.

The same heat flux must travel through all layers of a system in thermal equilibrium. If we assume heat flux through the relatively highly insulating mask wall is negligible and the CTS is opaque in the thermal IR then equations 5 and 6 may be used to determine heat flux through both the CTS and cellular shade layers of the system. The measured thermal conductivity of the CTS foam, k_{CTS}, foam thickness, L_{CTS}, and measured temperatures, $T_{CTS\_cold/warm}$, on either side of the CTS are all required. The derived performance characteristics (such as heat flux and surface coefficients) were calculated for each grid area, A, and then summed over the entire specimen area to determine the overall performance of the system. Heat flux, q, was then calculated by dividing by the total specimen surface area.

$$Q = \frac{k_{CTS}}{L_{CTS}} \sum A \left(T_{CTS\_warm} - T_{CTS\_cold}\right) \quad [5]$$

$$q = \frac{Q}{A_{total}} \quad [6]$$

3. Design of the Experiment

Three measurement parameters were investigated in depth; inside-to-outside temperature differential, shade-to-window gap depth, and side (left/right) gap-width dimensions. The ranges of these parameters are listed in Table 1. Thirteen different cellular shades representing currently available products on the market were examined through the range of these three measurement parameters. A total of 94 different combinations of the three parameters and thirteen shades was measured and simulated using the simplified simulation model in Berkeley Lab WINDOW.

Table 1. Measurement parameters for perimeter gap investigation

Variable	Parameter	Set points	Unit
T_c	Cold side Temperature	-18, -10	°C
d_{gap}	Shade-window gap depth	3.0, 12.7, 25.4	mm
d_s	Side (d_{left} and d_{right}) gap width	0, 3, 12.7	mm

Eight single-cell, two cell-in-cell, two cell-in-cell-in-cell, and one stacked-double-cell were characterized. The average cell height, p, was calculated from the total height of the tested shade divided by the number of cells. The width, w, was then calculated from the cell height, measured side length, l_{s1}, and glue line length, l_{g1}. Material properties shown in Table 3 were measured normal to the material and assumed constant under the experimental conditions of this work.

The total hemispherical emissivity of cellular shade materials was directly measured according to ASTM C 1371-15 (ASTM 2015). It is possible to measure both the IR transmittance (T_{ir}) and emissivity of non-opaque samples through measurement of the sample on two different opaque backing surfaces (Devices 1981). The measured emittance, E_a, in each case is given by equation 7.

$$E_a = E_s + T_s\left(1 - T_s\frac{1-E_b}{1-(1-E_s-T_s)(1-E_b)}\right) \quad [7]$$

where E represents emittance, T transmittance, index s denotes sample, and b backing material. By doing this for two known backing materials with a large difference, the system of two equations can be used to solve for T_s and E_s. No simple closed solution to the system of two equations exists, so an iterative solution is applied.

A spectrophotometer was used to measure visible specular transmittance of the materials, which has been shown in previous studies to accurately represent the ratio of open area to material area, or thermal openness (Hart 2017).

The geometry for each cellular shade is listed in Table 2. When two materials are listed under a single Material ID, the first ID is room-side and the second is glass-side. The front properties face outward from the center of the cell and the back properties face inward towards the cell cavity.

Table 2. Cellular shade geometry and materials

				l_{g1}		l_{s1}		l_{s2}		l_{s3}	
ID	type	p [mm]	w [mm]	length [mm]	material ID	length [mm]	Material ID	length [mm]	material ID	length [mm]	material ID
CS01	single	25.1	22.4	6.7	CSM02	14.8	CSM01/CSM03				
CS02	single	23.4	24.1	7.9	CSM05	14.2	CSM04/CSM06				
CS03	single	25.7	20.0	7.9	CSM07	14.2	CSM08				

CS04	stacked double	15.6	13.5	1.5	CSM09	9.8	CSM10	12.7			
CS05	single	21.4	26.6	7.9	CSM11	14.2	CSM12				
CS06	single	28.6	33.1	7.9	CSM13	19.1	CSM14				
CS07	cell-in-cell	25.7	35.1	8.8	CSM16	18.4	CSM17	16.2	CSM18		
CS08	cell-in-cell	23.9	36.8	8.8	CSM19	18.4	CSM17	16.2	CSM19		
CS09	single	24.5	36.2	7.0	CSM20	19.1	CSM20				
CS10	single	20.2	39.6	5.3	CSM21	19.9	CSM21				
CS11	single	27.8	32.7	7.6	CSM22	18.7	CSM22				
CS12	cell-in-cell-in-cell	44.7	62.7	11.2	CSM16	34.1	CSM17	26.4	CSM18	24.1	CSM23
CS13	cell-in-cell-in-cell	44.7	62.7	11.2	CSM19	34.1	CSM17	26.4	CSM18	24.1	CSM19

Table 3. Cellular shade material properties. Materials with lowe coating are identified.

Material ID	Emissivity Front [-]	Emissivity Back [-]	T_{ir} [-]	Openness [-]
CSM01	0.70	0.68	0.16	0.03
CSM02	0.75	0.78	0.06	0.00
CSM03	0.65	0.63	0.19	0.05
CSM04	0.65	0.66	0.23	0.19
CSM05	0.70	0.66	0.14	0.19
CSM06	0.67	0.69	0.11	0.01
CSM07	0.78	0.78	0.00	0.00
CSM08	0.69	0.69	0.11	0.00
CSM09	0.71	0.74	0.07	0.00
CSM10	0.67	0.74	0.08	0.00
CSM11	0.50	0.50	0.04	0.00
CSM12	0.81	0.57	0.00	0.00
CSM13	0.54	0.50	0.08	0.00
CSM14	0.78	0.54	0.01	0.00
CSM15	0.71	0.56	0.56	0.00
CSM16	0.78	0.78	0.03	0.00
CSM17	0.72	0.72	0.12	0.01
CSM18	0.68	0.68	0.14	0.02
CSM19	0.78	0.04 (lowe)	0.00	0.00
CSM20	0.69	0.69	0.19	0.02
CSM21	0.84	0.04 (lowe)	0.00	0.00
CSM22	0.37	0.37	0.58	0.59
CSM23	0.17	0.17	0.71	0.00

3.1. Boundary conditions

The ISO 15099 flat plate correlations for natural convective surface-to-air heat-transfer coefficient on vertical surfaces were utilized to determine room side convection in this work. Forced convection on the cold side is very complicated to characterize locally since the as-tested geometry is somewhat complex and the flow is turbulent. The most accurate

match of simulation to the measured conditions was therefore achieved by assigning an area-weighted average of the measured local combined surface heat-transfer coefficient in the simplified model. The cold side surface heat-transfer coefficient was calculated similar to Equations 5 and 6 from the local heat flux and the temperature difference between the CTS surface and the cold-side air temperature. The surface coefficient was kept sufficiently large, at 23 ± 5 $Wm^{-2}K^{-1}$ that its resistance was typically less than 5 ± 1 percent of the overall system resistance. The resistance could not be neglected but small deviations in the assigned numerical coefficient from the as-tested conditions had minor impact to the simulated overall system performance. A summary of boundary conditions is presented below. These boundary conditions were the set points for experiments and are therefore nominal values. The actual measured values were used as inputs for the simulations.

- Warm side: $T_w = 21$ °C
  Radiation coefficient - surface to ambient temperature (T_w)
  Convection coefficient – ISO 15099 flat plate model
- Cold side: $T_c = -18$ °C or -10 °C
  Combined radiation and convection to ambient temperature (T_c)

4. Results and analysis

Three methods, as outlined above, were used to compare several representative cellular shade configurations to assess the accuracy of the ISO 15099 approximations. Generalized convection in cavities and over cellular shade surfaces were first studied to gain insight into expected deviations from current models. The measured and simulated heat flux through cellular shades in the as-tested configurations was subsequently compared to quantify the accuracy of the simplified model.

The relative heat flux difference between methods was used as an error metric to compare methods and was calculated as:

$$E = \frac{q_1 - q_2}{q_1} \qquad [8]$$

The relative heat flux difference was used en lieu of an absolute metric because the range of measurement parameters resulted in large variations in heat flux between individual configurations.

4.1. General sealed cavities

Detailed FEA was used to determine the heat flux through the geometries shown in Figure 3 for a wide range of temperatures. The simulations were performed non-dimensionally per equations 1-3 in order to generalize the solutions. The resulting steady state heat flux, represented here by Nu (equation 1), is determined and plotted against Ra (equation 2).

Table 4 shows the laminar flow numerical solutions of Nu for an AR=1 isothermal wall cavity. The current work benchmarks well with previous studies presented in Barakos et al. (1994). There is a large error between ISO 15099 (2003) and all other studies. This discrepancy is due to an error within the ISO 15099 model that affects all solutions when AR is greater than ½ and less than 5, as previously shown by Gustavsen (2001).

Table 4. Comparison of Nusselt number (Nu) vs Rayleigh number (Ra) solutions for an isothermal wall AR=1 cavity from this work with previous works in literature (Barakos et al. 1994).

	Nu (% difference from current work)					
Ra	**current work**	**Barakos et al.**	**Markatos and Pericleous**	**De Vahl Davis**	**Fusegi et al.**	**ISO 15099**
10^3	1.118	1.114 (0.3%)	1.108 (0.9%)	1.118 (0.0%)	1.105 (1.1%)	1.011 (10%)
10^4	2.247	2.245 (0.1%)	2.201 (2.1%)	2.243 (0.2%)	2.302 (-2.4%)	1.424 (45%)
10^5	4.545	4.510 (0.8%)	4.43 (2.6%)	4.519 (0.6%)	4.646 (-2.2%)	4.534 (0.2%)
10^6	8.954	8.806 (1.7%)	8.754 (2.3%)	8.799 (1.7%)	9.012 (-0.6%)	11.275 (-23%)

Figure 8 shows the correlation between the current FEA simulations and ISO 15099 for rectangular and hexagonal cells at AR of 0.5 and 1. The divergence between the models, due to the previously described error in ISO 15099, shows that we should anticipate a significant under-prediction of the cellular shade Nu, and in turn, system heat flux in some cases. The error is greatest, up to 60 percent, when Ra is smallest, principally with smaller cells and low temperature difference between cell walls.

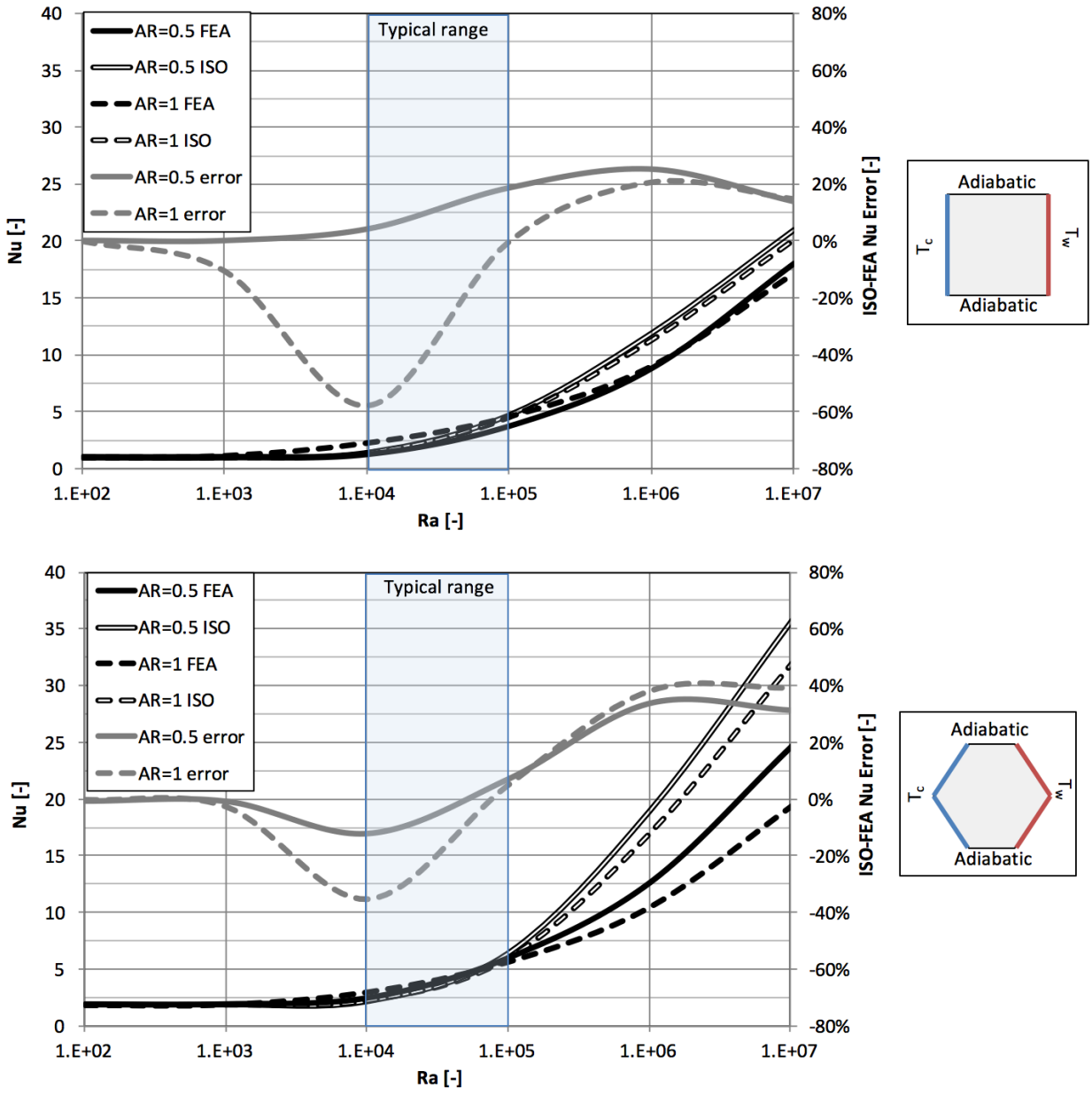

Figure 8. Nu = f(Ra) correlation curves solved by FEA of cell geometries at height-to-width aspect ratios (AR) of 0.5 and 1 compared to ISO 15099 (2003). The typical Ra range encountered during measurements is highlighted.

Correlations for heat flux in high AR cavities, such as those formed between cellular shades and glazing are shown in Figure 9. The current work shows that wave-type surfaces of cellular shades have little impact, less than 2 percent, on heat flux through these cavities. Similarly, the impact of wave-type surface on natural convection of room-side of cellular shades is shown in Figure 10 to be relatively small at less than 5 percent. The wave

geometry shown was based on a typical length and pitch equal to $0.25d_{gap}$. The expected error for these configurations also appears to be significant, but offsetting, to the expected error from the cell cavity models.

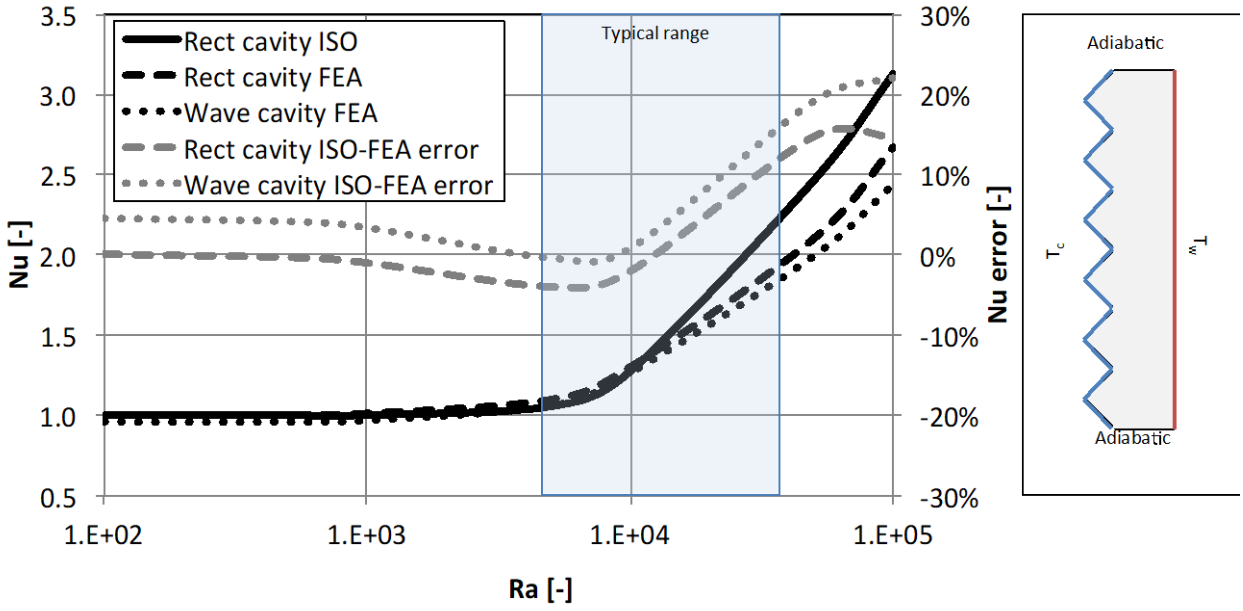

Figure 9. Nu = f(Ra) correlation curves solved by FEA for rectangular (flat wall to flat wall) and wave (wave wall to flat wall) cavities at AR=40 compared to ISO 15099 (2003). The typical Ra range encountered during measurements is highlighted.

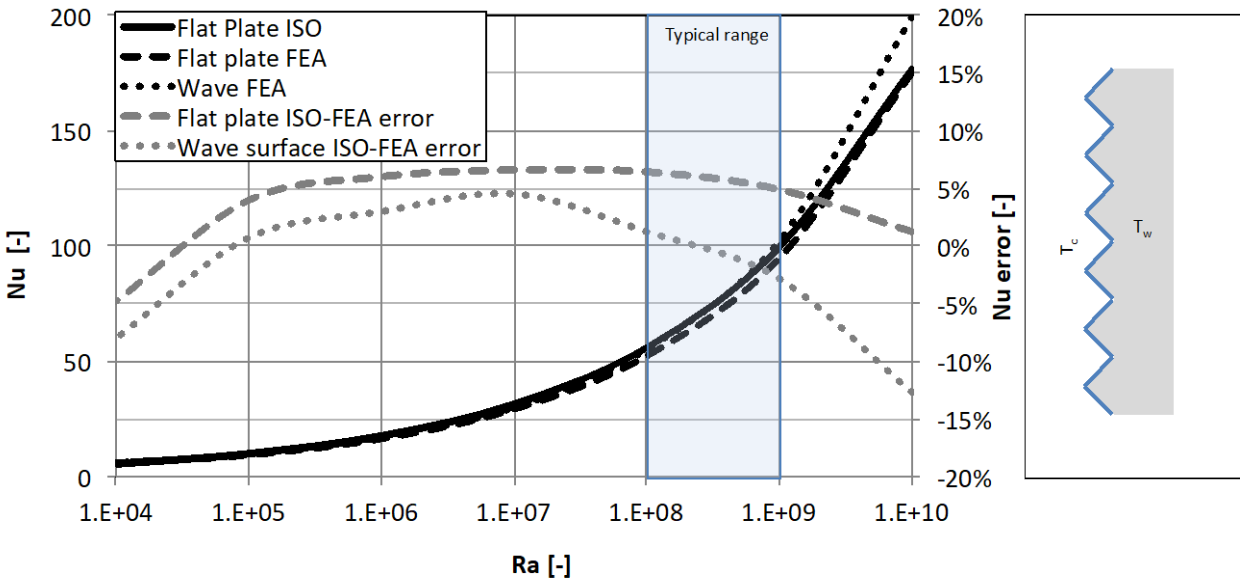

Figure 10. Nu = f(Ra) correlation curves solved by FEA of natural convection on vertical flat plate and wave surfaces ($l = p = 0.25d_{gap}$) compared to ISO 15099 (2003). The typical Ra range encountered during measurements is highlighted.

4.2. As-tested

4.2.1. Baseline

Test configurations with one and two CTS's, where the second CTS replaces the cellular shade in Figure 7, were used to obtain a baseline comparison between measured and simulated heat flux. Figure 11a shows a comparison between measured heat flux and Berkeley Lab WINDOW simulated heat flux for 15 baseline test cases. Perfect agreement between methods would result in a data point falling on the line of symmetry, with the 5% and 10% errors relative to the measured performance shown for reference. The calculated uncertainty of each measurement is shown with vertical error bars on each data point. The coefficient of determination, R^2, relative to the line of symmetry and linear fit between the measured and simulated heat fluxes for the single CTS data set is also shown. Figure 11b presents the distribution of the percent difference between measured and simulated heat fluxes. This plot is used to identify systematic errors or biases between the methods.

Agreement between measured and simulated heat flux for all baseline cases is within the calculated error of the measurements. Figure 11b shows the data falling into two general groups at approximately one percent and two percent relative heat flux differences.

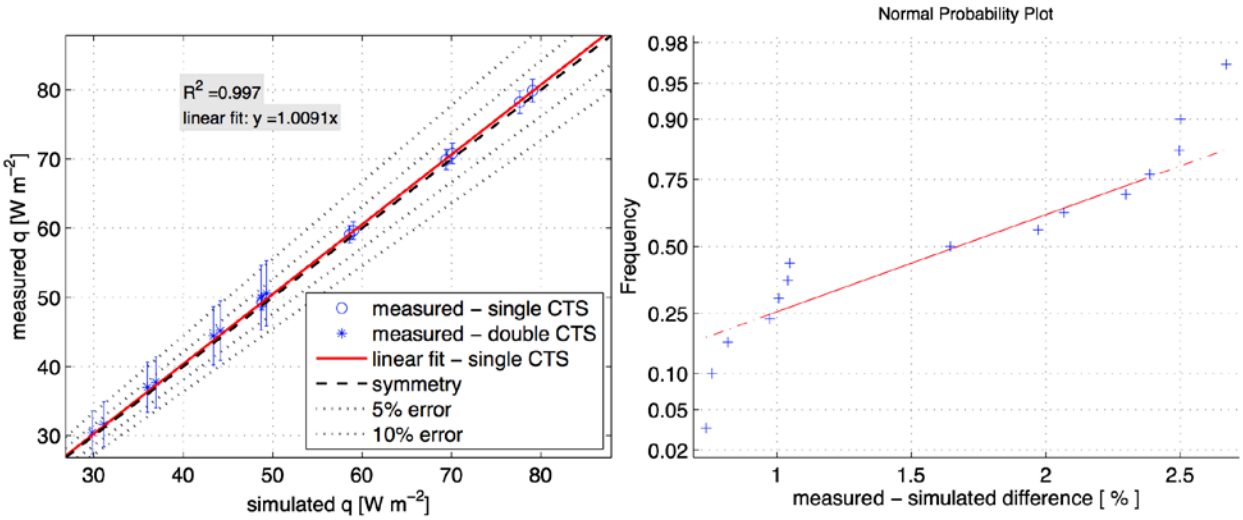

Figure 11. a) Measured to simulated heat flux comparison for CTS baseline measurements. A linear fit to the single CTS measurements is provided. b) Cumulative probability distribution of the percent difference between measured and simulated data. Coefficient of determination, R^2, is relative to line of symmetry.

Detailed parameters, including surface temperatures and heat flux by layer, are presented in Table 5 to better understand the sources of the heat flux differences and groupings shown in Figure 11. Single CTS measurements had an average measurement to simulation

heat flux difference of 0.9%, with double CTS measurements at 2.3%. These averages account for the two groupings in Figure 11b. The source(s) of 0.9% single CTS average difference is unknown but is shown to be a consistent systematic bias that should be taken into account when correlating the cellular shade model to measured results.

The 1D Berkeley Lab WINDOW simulation required heat flux through the window and shade CTS's to be equal. In the measurements though this assumption was invalid as some energy was transferred through the mask wall on the cavity perimeter. This energy loss is most likely the primary source of the increased difference in heat flux with the double CTS configuration. The observation is supported by the larger measured-to-simulated heat flux error across the shade CTS, q_s, than the window CTS, q_w.

Table 5. Comparison of measured to simulated U-factors for sealed cavity CTS. Mean error of 10 measurements presented for each group.

	Window CTS				Shade CTS				
Group	T_{w_cold} [% diff]	T_{w_warm} [% diff]	h_{cold} [% diff]	q_w [% diff]	T_{s_cold} [% diff]	T_{s_warm} [% diff]	h_{warm} [% diff]	q_s [% diff]	U-factor [% diff]
Single CTS	0.15%	0.01%	-	0.91%	-	-	-	-	0.91%
Double CTS	0.11%	0.09%	-	2.26%	1.25%	1.49%	-	9.70%	2.26%

4.2.2. Cellular Shades

Figure 12a shows the initial comparison between Berkeley Lab WINDOW simulation and measured heat flux for all 94 measured cellular shade combinations. Analysis was performed on the basis of heat flux in lieu of thermal transmittance (U-factor) since heat flux is used in Berkeley Lab WINDOW for simulation convergence. This way it was possible to perform a quantitative correlation between the measured and simulated values in an attempt to validate the model.

The average simulated heat flux was approximately 5 percent less than measured, with a typical spread of ±8 percent. There were several cases though where the simulation largely overestimated heat flux, by as much as 16 percent. A detailed statistical analysis of the data was performed to determine if all measurements were valid and if the Berkeley Lab WINDOW simulation accurately represented measured performance for all tested configurations.

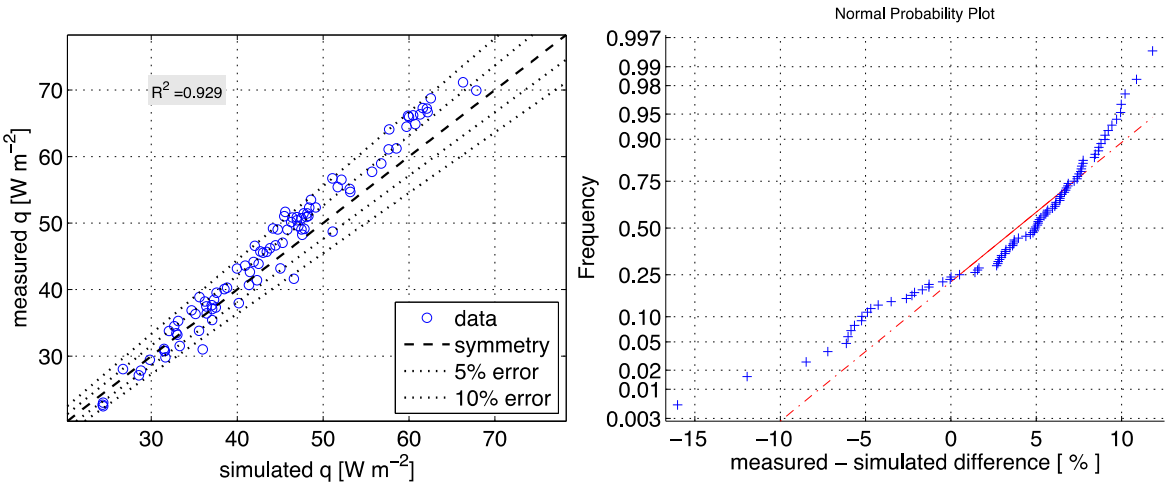

Figure 12. Measured to simulated heat flux comparison for 94 cellular shade configurations. Coefficient of determination, R^2, is relative to line of symmetry.

An analysis of variance (ANOVA) on the percent difference between the measured and simulated heat flux was performed and is presented in Figure 13 with a box plot. Parameters studied include the warm-cold side temperature difference, DT; side gap width, d_s; shade-window gap depth, d_{gap}; and the presence of low-e coating within the cellular shade, lowe (as identified in Table 3). The box plot compactly shows key information. The plot identifies the mean through the red center line, the 25 and 75 percent quartiles through the top and bottom edges of the box, the 95 percent confidence interval of the mean through the notched lines going out from the mean, the range of included data through the dashed line "whiskers", and finally it identifies outliers with red pluses. A data-point was considered an outlier if it was more than 1.5 times the interquartile range from either quartile.

Similar to Figure 12, Figure 13 shows that the mean heat flux difference for all data was 5 percent. This trend holds for most data groupings with significant biases when d_{gap} was set to the minimum achievable depth, and d_s=0 (sealed cavity).

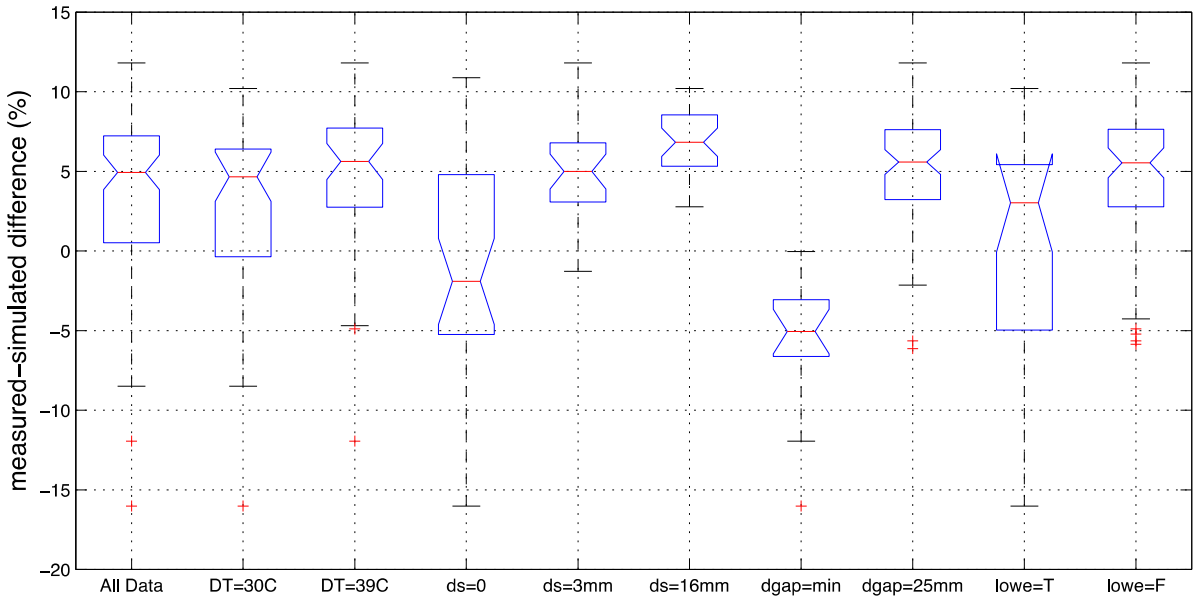

Figure 13. Box plot of measured to simulated difference in heat flux of the 94 shade combinations grouped by warm-cold side temperature difference, DT; side gap width, d_s; shade-window gap depth, d_{gap}; and the presence (True or False) of low-e coating within the cellular shade, lowe.

There are several potential drivers for the poor correlation between simulation and measured performance when d_{gap} was at the minimum, i.e. distance between head mounting rail and glazing, d_h, was zero (see Figure 14b). We believe the primary driver of poor correlation is that cellular shades do not hang with the commonly assumed average cell pitch, p, as determined based on the number of cells over the height of a shade layer. Typically, the top most cells are significantly stretched due to the weight of cells below and correspondingly the bottom cells lie nearly flat, as shown in Figure 14a. This scenario resulted in a variable d_{gap}. In the majority of test configurations d_{gap} was large (>25mm) resulting in low d_{gap} sensitivity. Window heat flux was sensitive to d_{gap} when d_h was at its minimum though. A revised method to calculate d_{gap} (equation 9) is proposed as d_{gap*} in equation 10. It is based on the midpoint between fully extended and fully flat cells. The geometry is described in Figure 14b.

$$d_{gap} = d_h + \frac{w_h - l_{g1}}{2} - \sqrt{{l_{s1}}^2 - \left(\frac{p}{2}\right)^2} \quad [9]$$

$$d_{gap*} = d_h + \frac{w_h - l_{g1} - \sqrt{{l_{s1}}^2 - \left(\frac{p}{2}\right)^2}}{2} \quad [10]$$

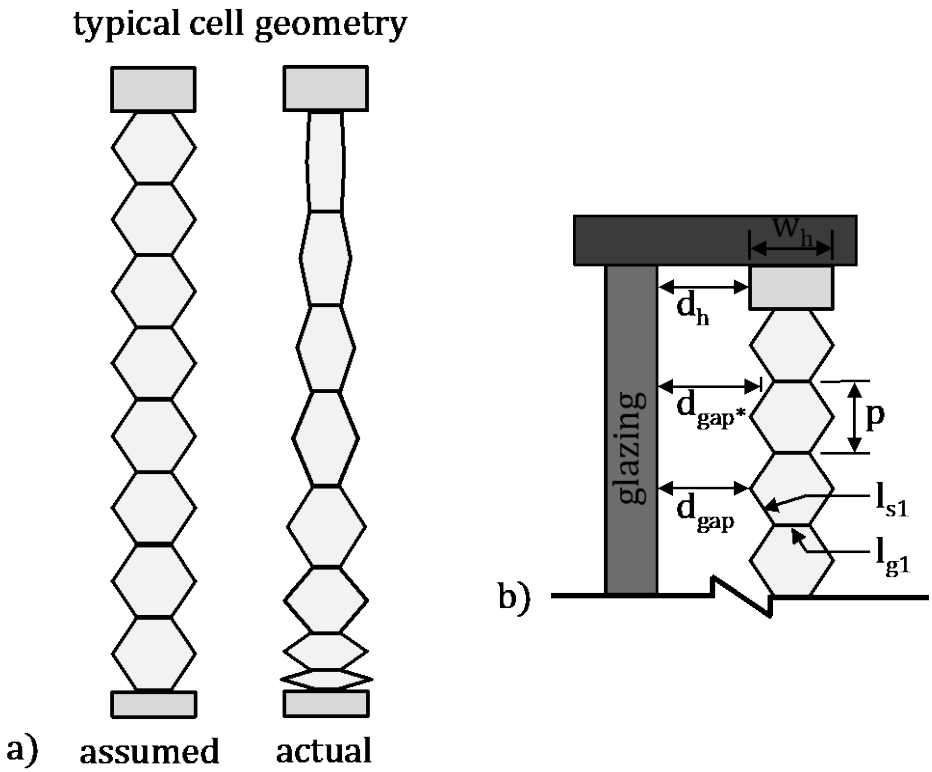

Figure 14. (a) End view of the assumed and actual cellular shade geometry when mounted to a window. (b) Geometry defining the distance from glazing surface to cellular shade, where p is the average cell pitch.

The cellular shades were mounted for measurements with their manufacturer supplied head and sill hardware. Profiles of this hardware, along with significant dimensions, are provided in Figure 15. CS01–CS06 utilized mounting hardware grouped into g1, and CS07–CS13 utilized mounting hardware grouped into g2. All hardware was constructed of aluminum extrusion with thermal conductivity of 160 $Wm^{-1}K^{-1}$. The significant area and relatively high thermal conductivity of this hardware must be considered for its thermal impact.

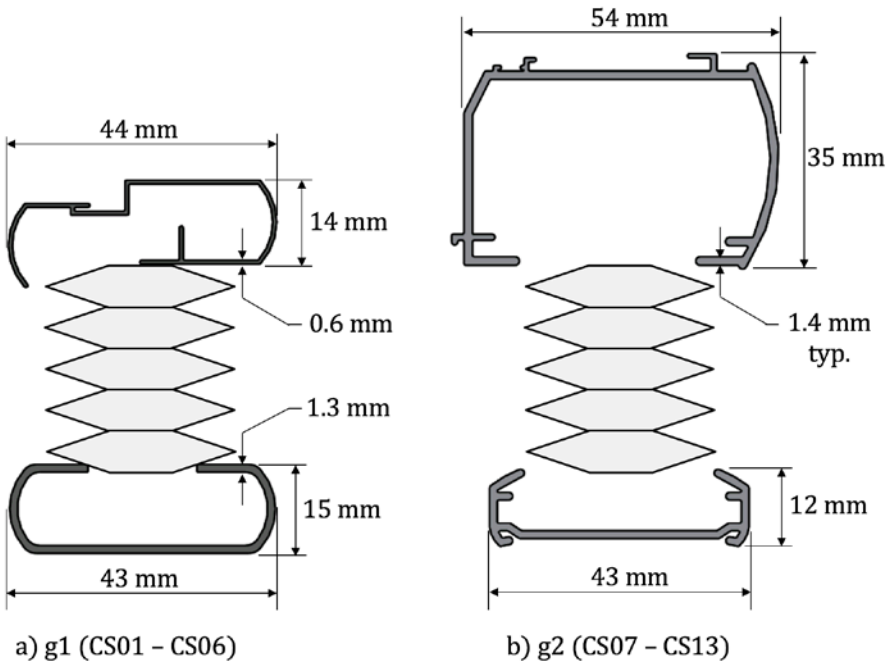

Figure 15. Profile view of extruded aluminum cellular shade mounting hardware with significant dimensions. a) CS01–CS06 mounting hardware (g1), and b) CS07–CS13 mounting hardware (g2).

Viewing the same initial correlation data shown in Figure 13, but regrouped in Figure 16 by individual product and cellular shade mounting type (g1 and g2) reveals a significant 5.8 percentage point difference in correlation between the two mounting types. The shades are all similar so the variations in mounting hardware are the most likely source of the difference. The thermal effect of mounting hardware as shown in Figure 1e with head and sill rails cannot be ignored. The bias introduced by the mounting hardware was addressed by FEA simulations of each measured test case with and without mounting hardware. A correction factor for the simulated results was then determined based on the percent difference in total heat flux between the two models.

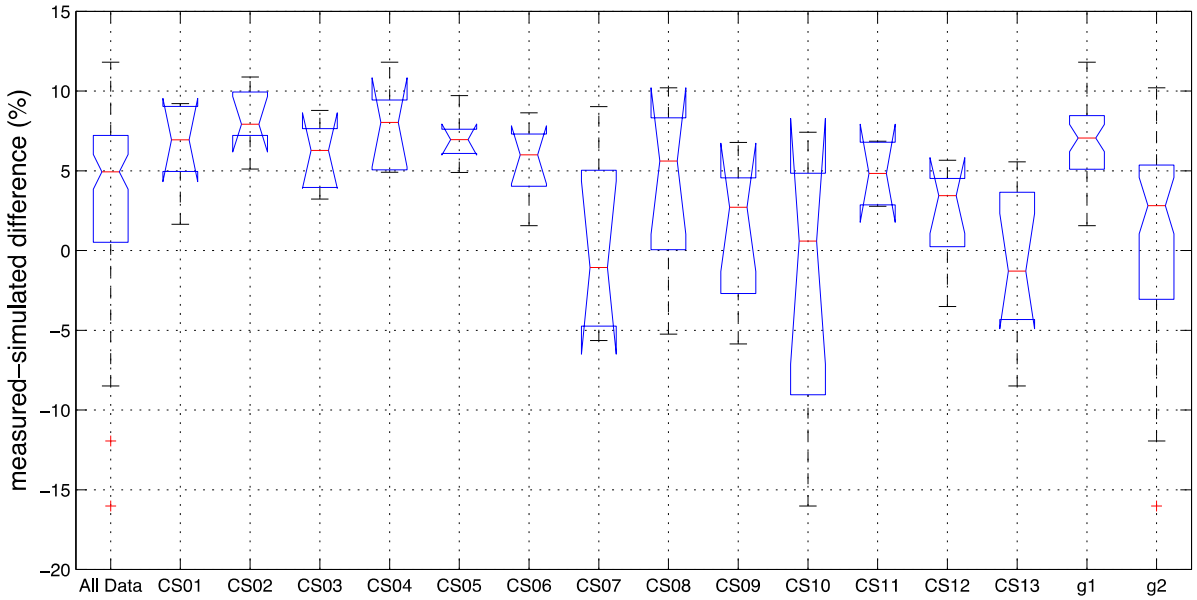

Figure 16. Box plot of measured to simulated difference in heat flux grouped by product, CS01-CS13, and cellular shade mounting type, g1 (CS01-CS06) and g2 (CS07-CS13).

The three noted corrections were applied to the initial simulation results in the following order:

- d_{gap*} was calculated to replace d_{gap} and all simulations were recalculated
- The resulting simulated heat flux was multiplied by 1.0091 to account for the average 0.91 percent error between measurement and simulation seen in the CTS calibration
- Each revised simulated heat flux was multiplied by the FEA simulated percent error in heat flux between configurations with and without shade mounting hardware.

The resulting comparison between the revised Berkeley Lab WINDOW simulation and measured heat flux for all combinations is shown in Figure 17. The revised measured to simulated heat flux difference is 0.5 percent, with a typical spread of ±6 percent.

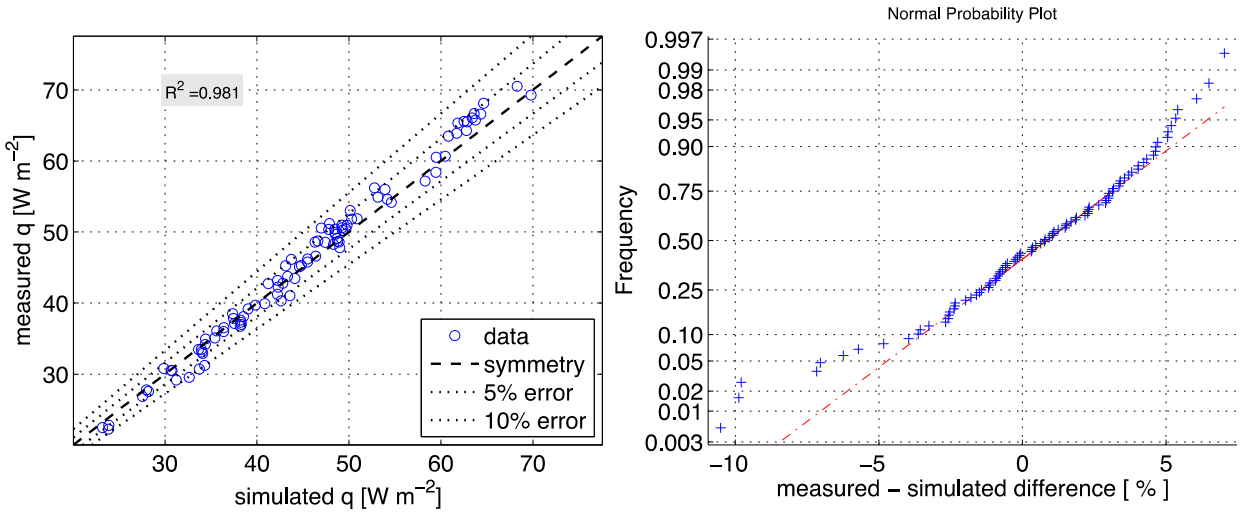

Figure 17. Measured to simulated heat flux comparison for 94 cellular shade configurations based on data corrected for CTS measurement error and cell shade mounting hardware. Coefficient of determination, R^2, is relative to line of symmetry.

Applying the revised d_{gap^*} calculation reduced the difference between d_{gap}=min and d_{gap}=25mm from 10 percentage points to 3 percentage points, as shown in Figure 18. The performance of d_{gap}=min became in line with results for d_s=0 (sealed side walls). Since all d_{gap}=min cases tested were with d_s=0 the error associated with d_{gap} was therefore eliminated. The remaining unresolved significant error is the 3-percentage point difference between d_s=0 and d_s=16mm configurations. This is the same correlation difference seen with side gaps in Hart (2015a) when compared to all other measurements, indicating that the difference is most likely due to inaccuracy of the ISO 15099 model and not the implementation of the model with cellular shades.

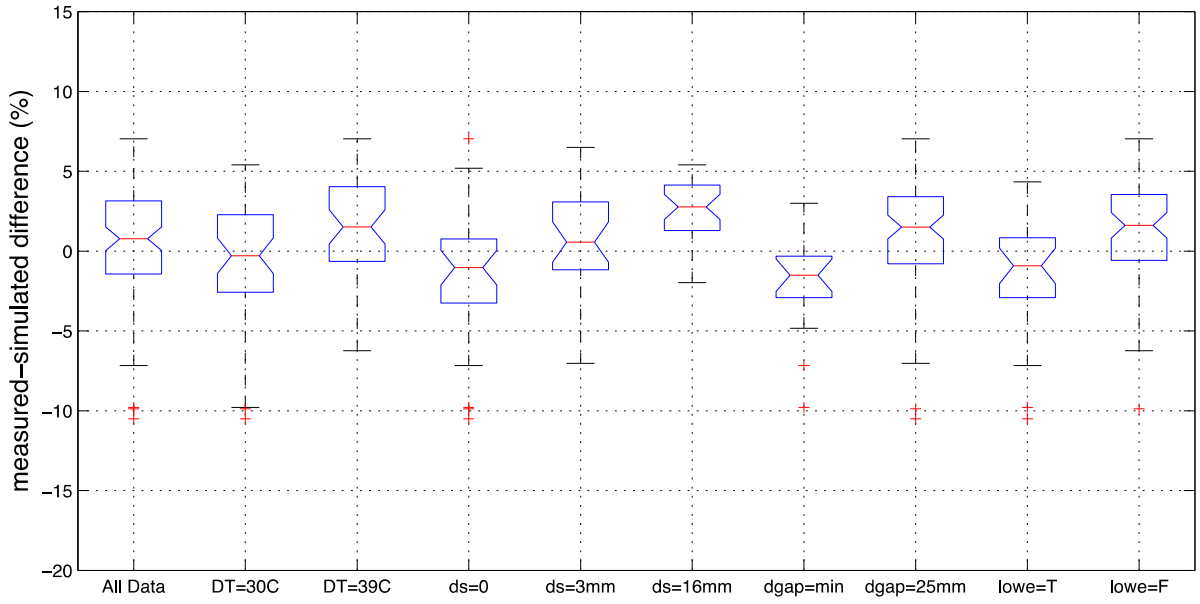

Figure 18. Box plot of revised measured – WINDOW simulated difference in heat flux grouped by warm-cold side temperature difference, DT; side gap width, d_s; shade-window gap depth, d_{gap}; and the presence (True or False) of low-e coating within the cellular shade, lowe.

Based on the FEA simulations, the average impact of the g1 mounting hardware was a 3.6 percent increase in simulated heat flux, with a 3.2 percent increase for g2. Applying this correction, along with the other two corrections previously stated, brought the two groups from a 5.8 percentage point difference in average heat flux to a 3.0 percentage point difference. The results are shown in Figure 19. The revised simulations did not fully reconcile the performance difference so it's probable there are additional significant aspects of the mounting hardware, such as air leakage, yet unaccounted for.

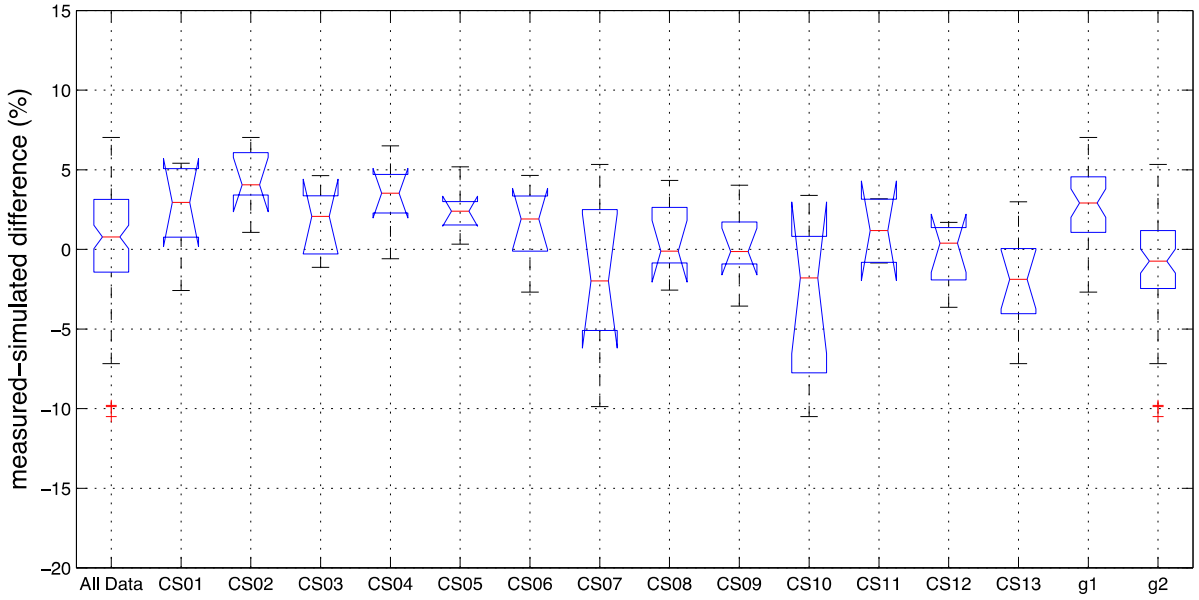

Figure 19. Box plot of revised measured to simulated difference in heat flux grouped by product, CS01-CS13, and cellular shade mounting type, g1 (CS01-CS06) and g2 (CS07-CS13).

5. Conclusions

The impact on zero-solar-load thermal transmittance of window systems with cellular shades was measured, simulated using CFD analysis, and simulated utilizing simplified correlations from ISO 15099 as implemented in Berkeley Lab WINDOW and THERM software.

CFD analysis was performed for ranges of Rayleigh numbers typically encountered inside cellular shades. The results show ISO 15099 typically underestimates heat flux, up to 60 percent, for AR = 1 rectangular cavities and overestimates heat flux, up to 20%, for AR = 0.5 rectangular cavities. Heat flux in high AR cavities, such as those formed between cellular shades and glazing, has been demonstrated in previous studies to be over-predicted by ISO 15099. The current work showed that wave-type surfaces of cellular shades have little impact, less than 2 percent, on heat flux through these cavities. Similarly, the impact of wave-type surface on natural convection of room-side of cellular shades was shown to be relatively small at less than 5 percent.

Based on 94 unique steady-state measurements of 13 cellular shade products that encompasses the majority of room-side mounted cellular shades in the market, the simulation method used by Berkeley Lab WINDOW was shown to accurately represent heat flux of measured configurations to a mean relative error of 0.5 percent with a standard deviation of 3.8 percent. A shade-to-glass gap depth based on the midpoint between fully extended and fully flat cells was used. Several shade parameters have significant influence on correlation accuracy, including the distance between shade and glass, the inconsistency in cell stretch from top to bottom, the openness of the cell walls, the size of perimeter gaps, and the mounting hardware.

The author was unable to find comparable experimental or simulation results in the literature for cellular shading systems. Thermal transmittance was studied exclusively in this work; a solar heat gain model for these products will be studied and validated in the future.

6. Acknowledgements

This work was supported by the Assistant Secretary for Energy Efficiency and Renewable Energy, Building Technologies Program, of the U.S. Department of Energy under Contract no. DE-AC02-05CH11231.

7. References

ASTM International. (2014). C1199-14 Standard Test Method for Measuring the Steady-State Thermal Transmittance of Fenestration Systems Using Hot Box Methods. West Conshohocken, Pa.

ASTM International. (2015). C1371-15 Standard Test Method for Determination of Emittance of Materials Near Room Temperature Using Portable Emissometers. West Conshohocken, Pa.

ASTM International. (2017). C518-17 Standard Test Method for Steady-State Thermal Transmission Properties by Means of the Heat Flow Meter Apparatus. West Conshohocken, Pa.

Barakos, G., Mitsoulis, E. and Assimacopoulos, D. (1994). *Natural convection flow in a square cavity revisited: Laminar and turbulent models with wall functions.* Int. J. Numer. Meth. Fluids, 18: 695–719.

Bejan, A. (2004). Convection Heat Transfer. 3rd ed. John Wiley & Sons, Inc.

Chenoweth, D.R. and Paolucci, S. (1986). Natural convection in an enclosed vertical air layer with large horizontal temperature differences. Journal of Fluid Mechanics, 169:173-210.

Collins, M., & Wright, J. L. (1998). Calculating Center-Glass Performance Indices of Windows with a Diathermanous Layer. *ASHRAE Transactions 112*, 1–12.

Devices and S. Co., (1981). Use of emissometer for semi-transparent materials measurements. Tech. rep., D&S Technical Note 81-1.

Dijk, D. Van, & Oversloot, H. (2003). WIS, the European tool to calculate thermal and solar properties of windows and window components. *Proceedings of Building Simulation*, 259–266.

Dodge, L. (2011). *Thermal Insulating Value of Cellular Shades With and Without Side Seals.* Lee G. Dodge Residential Energy Laboratory Salida, Colorado.

El Sherbiny, S.M., G.D. Raithby, and K. Hollands. (1982). Heat Transfer by Natural Convection Across Vertical and Inclined Layers. ASME Journal of Heat Transfer 104: 96-102.

Gustavsen, A. (2001). Heat transfer in window frames with internal cavities. Ph.D. dissertation, Department of Building and Construction Engineering. Norwegian University of Science and Technology, Trondheim, Norway.

Hart, R., H. Goudey, & D.C. Curcija (2017): Experimental validation and model development for thermal transmittances of porous window screens and horizontal louvred blind systems, Journal of Building Performance Simulation, 1-15. https://doi.org/10.1080/19401493.2017.1323010

International Organization for Standardization 12567-1. (2010). Thermal performance of windows and doors -- Determination of thermal transmittance by the hot-box method -- Part 1: Complete windows and doors. Geneva, Switzerland.

International Organization for Standardization 15099. (2003). Thermal Performance of Windows, Doors, and Shading Devices—Detailed Calculations. Geneva, Switzerland.

Laouadi, A. (2009). Thermal performance modeling of complex fenestration systems. *Journal of Building Performance Simulation*, *2*(3), 189–207.

Oosthuizen, P. (2011). *Natural Convective Heat Transfer from an Inclined Isothermal Plate with a Wavy Surface*. 42nd AIAA Thermophysics Conference. Honolulu, Hawaii. Paper AIAA 2011-3943

Oosthuizen, P. and J.T. Paul. (2012). *A Numerical Study of the Convective Heat Transfer Rate from a Window Covered by a Slatted Top Down-Bottom Up Blind System to an Adjacent Room.* Proceedings of the 20th Annual Conference of the CFD Society of Canada, Canmore AB, May 9-12.

Petersen, J., G. Sullivan, K. Cort, M. Merzouk, J. Weber. (2015). *Evaluation of Cellular Shades in the PNNL Lab Homes.* Pacific Northwest National Laboratory Richland, Washington

Steven Winter Associates, Inc. (2008). *Insulating Window Shade Evaluation: Quantifying the Benefits of Double Honeycomb Shades with Air-Sealing Side Tracks.* Steven Winter Associates, Inc.

Tarcog: Mathematical Models for calculation of thermal performance of glazing systems with or without shading Devices. (2006). Carli, Inc.

Wright, J.L. (1996). A Correlation to Quantify Convective Heat Transfer Between Vertical Window Glazings. ASHRAE Transactions 102 (1).

Wright, J. L. (2008). Calculating Center-Glass Performance Indices of Glazing Systems with Shading Devices. ASHRAE Transactions, 114(2), 199–209.

Yao, L. S. (1983). *Natural Convection along a Vertical Wavy Surface.* Journal of Heat Transfer 105, 465-468.

Zhao, Y., D. Curcija, J. Power, W. Goss. (1998). Improved Heat Transfer Correlations for Quantifying Laminar Natural Convection Across Fenestration Glazing Cavities. *Thermal Performance of the Exterior Envelopes of Buildings VII.* Clearwater Beach, FL.